Monthly Notices of the ROYAL ASTRONOMICAL SOCIETY

MNRAS **471,** 4374–4380 (2017) doi:10.1093/mnras/stx1862
Advance Access publication 2017 July 22

K2-113: a dense hot-Jupiter transiting a solar analogue

Néstor Espinoza,[1,2★] Markus Rabus,[1] Rafael Brahm,[1,2] Matías Jones,[3] Andrés Jordán,[1,2,4] Felipe Rojas,[1] Holger Drass,[1] Maja Vučković,[5] Joel D. Hartman,[6] James S. Jenkins[7] and Cristián Cortés[2,8]

[1]*Instituto de Astrofísica, Facultad de Física, Pontificia Universidad Católica de Chile, Av. Vicuña Mackenna 4860, 782-0436 Macul, Santiago, Chile*
[2]*Millennium Institute of Astrophysics, Av. Vicuña Mackenna 4860, 782-0436 Macul, Santiago, Chile*
[3]*European Southern Observatory, Alonso de Cordova 3107, Vitacura, Casilla 19001, Santiago 19, Chile*
[4]*Max-Planck-Institut für Astronomie, Königstuhl 17, Heidelberg 69 117, D-69117, Germany*
[5]*Facultad de Ciencias, Instituto de Física y Astronomía, Universidad de Valparaíso, Gran Bretaña 1111, Playa Ancha, Valparaíso 2360102, Chile*
[6]*Department of Astrophysical Sciences, Princeton University, NJ 08544, USA*
[7]*Departamento de Astronomía, Universidad de Chile, Camino al Observatorio 1515, Cerro Calán, Santiago, Chile*
[8]*Departamento de Física, Facultad de Ciencias Básicas, Universidad Metropolitana de la Educación, Av. José Pedro Alessandri 774, 7760197 Ñuñoa, 36-D Santiago, Chile*

Accepted 2017 July 19. Received 2017 July 19; in original form 2016 November 22

ABSTRACT

We present the discovery of K2-113, a dense hot-Jupiter discovered using photometry from Campaign 8 of the *Kepler*-2 (*K*2) mission and high-resolution spectroscopic follow-up obtained with the FEROS spectrograph. The planet orbits a $V = 13.68$ solar analogue in a $P = 5.817\,60^{+0.000\,03}_{-0.000\,03}$ d orbit, and has a radius of $0.93^{+0.10}_{-0.07} R_{\rm J}$ and a mass of $1.29^{+0.13}_{-0.14} M_{\rm J}$. With a density of $1.97^{+0.60}_{-0.53}$ g cm^{-3}, the planet is among the densest systems known having masses below 2 $M_{\rm J}$ and $T_{\rm eq} > 1000$, and is just above the temperature limit at which inflation mechanisms are believed to start being important. Based on its mass and radius, we estimate that K2-113 should have a heavy element content of the order of $\sim$110 $M_\oplus$ or greater.

Key words: planets and satellites: composition – planets and satellites: detection.

1 INTRODUCTION

Transiting extrasolar planets are one of the most precious systems to discover because they allow for a wide range of characterization possibilities. Combined with radial velocity (RV) or transit timing variation analysis, the mass of these systems can be extracted, which in turn allows us to compute their densities, an important measurement that sheds light on the composition of these distant worlds.

Despite their importance, only a small fraction ($\sim$10 per cent) of the currently $\sim$2500 known transiting extrasolar planets[1] are well suited for further characterization studies, mainly because the bulk of these discoveries have been made with the original *Kepler* mission (Borucki et al. 2010), whose stars are generally too faint and most of the planets too small to characterize. Although the bulk of the transiting extrasolar planets fully characterized to date come from ground-based transit surveys such as HATNet (Bakos et al. 2004), HATSouth (Bakos et al. 2013) and WASP (Pollacco et al. 2006), the search for transiting exoplanets around relatively bright stars has also benefited from the discoveries made by the repurposed *Kepler* mission, dubbed *K*2, which has allowed us to push discoveries even to smaller planets, with hundreds of new systems discovered to date[2] (see e.g. Crossfield et al. 2016, and references therein) and many more to come.

Among the different types of transiting extrasolar planets known to date, short-period ($P \lesssim 10$), Jupiter-sized exoplanets – the so-called hot-Jupiters – have been one of the most studied, mainly because they are the easiest to detect and characterize. However, these are also one of the most intriguing systems to date. One of the most interesting properties of these planets is their 'inflation', i.e. the fact that most of them are larger than what is expected from structure and evolution models of highly irradiated planets (Baraffe et al. 2003; Fortney, Marley & Barnes 2007). Although the inflation mechanism is as of today not well understood, at irradiation levels of about 2×10^8 erg cm^{-2} s^{-1} ($\sim$1000 K), evidence suggests it stops being important (Kovács et al. 2010; Demory & Seager 2011; Miller & Fortney 2011). Planets cooler than this threshold, which here we refer to as 'warm' Jupiters, appear on the other hand more compact than pure H/He spheres, which in turn implies an enrichment in heavy elements that most likely makes them deviate from the composition of their host stars (Thorngren et al. 2016).

★ E-mail: nespino@astro.puc.cl
[1] http://www.exoplanets.org, retrieved on 2016/11/19
[2] keplerscience.arc.nasa.gov

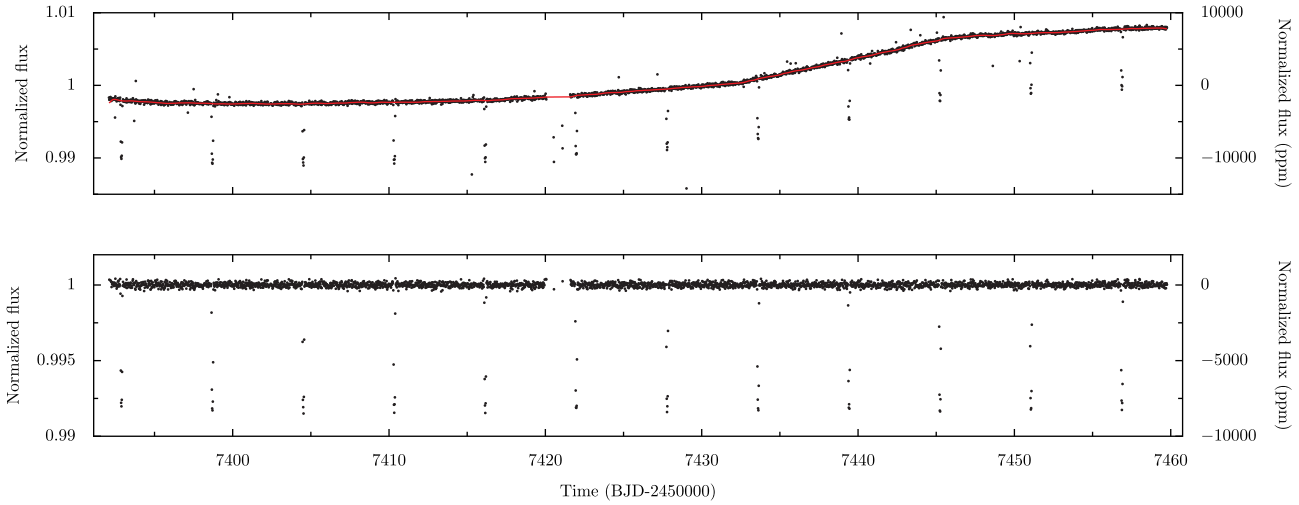

Figure 1. *Upper panel*. EVEREST photometry for the star EPIC 220504338 (black points) along with the 20-h median filter smoothed with a 3-h Gaussian filter (red line), which captures the intrinsic variability of the star. *Lower panel*. Photometry normalized with respect to our filter.

Here, we present a new planetary system that is in the 'hot' Jupiter regime, but whose structure resembles more that of a 'warm' Jupiter: K2-113, a planet ∼10 per cent smaller than Jupiter but ∼30 per cent more massive orbiting a star very similar to our Sun. The paper is structured as follows. In Section 2 we present the data, which includes photometry from Campaign 8 of the *K*2 mission and spectroscopic follow-up using the FEROS spectrograph. In Section 3, we present the analysis of the data. Section 4 presents a discussion and Section 5 our conclusions.

2 DATA

2.1 *K*2 photometry

The candidate selection for the photometry of Campaign 8 of the *K*2 mission was done as described in Espinoza et al. (2016). Briefly, the photometry is first normalized with respect to any long-term variation (either of instrumental and/or stellar nature) and candidates are selected using a Box Least Squares algorithm (BLS; Kovács, Zucker & Mazeh 2002). Here, we decided to obtain the photometry for the candidate selection using our own implementation of the EPIC Variability Extraction and Removal for Exoplanet Science Targets (EVEREST) algorithm described in Luger et al. (2016), due to its potential of conserving stellar variability (which we filter for our candidate selection with a 20-h median filter smoothed with a 3-h Gaussian filter, but which we also use in our analysis; see Section 3), although the full, final analysis performed here is done on the EVEREST light curve released at the Mikulski Archive for Space Telescopes (MAST) web site,[3] using the new updated method described in Luger et al. (2017). Our candidate selection procedure identified a planetary companion candidate to the star EPIC 220504338, with a period of ∼5.8 d and a depth of ∼7500 ppm. The overall precision of the light curve is ∼138 ppm; the photometry is shown in Fig. 1.

2.2 Spectroscopic follow-up

In order to confirm the planetary nature of our candidate, high-resolution spectroscopic follow-up was performed with the FEROS spectrograph (Kaufer & Pasquini 1998) mounted on the MPG 2.2-m telescope located at La Silla Observatory in August (three spectra) and November (six spectra) of 2016, in order to obtain both initial stellar parameters for the candidate stellar host and high-precision RV measurements. The spectra were obtained with the simultaneous calibration method, in which a ThAr calibration lamp is observed in a comparison fibre next to the science fibre, allowing us to trace instrumental RV drifts. The data were reduced with a dedicated pipeline (CERES; Jordán et al. 2014; Brahm, Jordán & Espinoza 2017a) which, in addition to the radial velocities and bisector spans (BIS), also calculates rough atmospheric parameters for the target star. This indicated the candidate host star was a G dwarf, with an effective temperature of $T_{\rm eff} = 5500 \pm 100$ K, surface log-gravity of $\log g_* = 4.2 \pm 0.3$ dex and a metallicity of [Fe/H] $= 0.2 \pm 0.1$ dex, all very much consistent with solar values.

The obtained RVs phased up nicely with the photometric ephemerides, hinting at a semi-amplitude of $\sim$140 m s^{-1}, consistent with an object of planetary nature (see Section 3). In addition, the measured BIS showed no correlation with the RVs, which is illustrated on Fig. 2; performing a Monte Carlo simulation by assuming that the errors on the RVs and BIS are Gaussian gives a correlation coefficient of $\rho = 0.15 \pm 0.16$, which is consistent with zero. The obtained radial velocities and BIS are presented in Table 1. These results prompted us to perform a full analysis of the system, which we present in the next section.

3 ANALYSIS

3.1 Stellar properties

In order to obtain the parameters of the host star, we first use the Zonal Atmospheric Stellar Parameters Estimator (ZASPE; Brahm et al. 2015, 2017b) algorithm. In brief, ZASPE compares the observed spectrum against a grid of stellar spectra in the most sensitive spectral zones to atmospheric parameters and determines the errors in the parameters by considering the systematic mismatch between the data and the models. In this case, we run ZASPE on a high-signal-to-noise (SNR; ∼100) spectrum that was generated by co-adding the nine individual FEROS spectra, which obtains a $T_{\rm eff} = 5627 \pm 88$ K, $\log g_* = 4.400 \pm 0.146$ dex, [Fe/H] $= 0.180 \pm 0.062$ dex and projected rotational velocity

[3] https://archive.stsci.edu/prepds/everest/

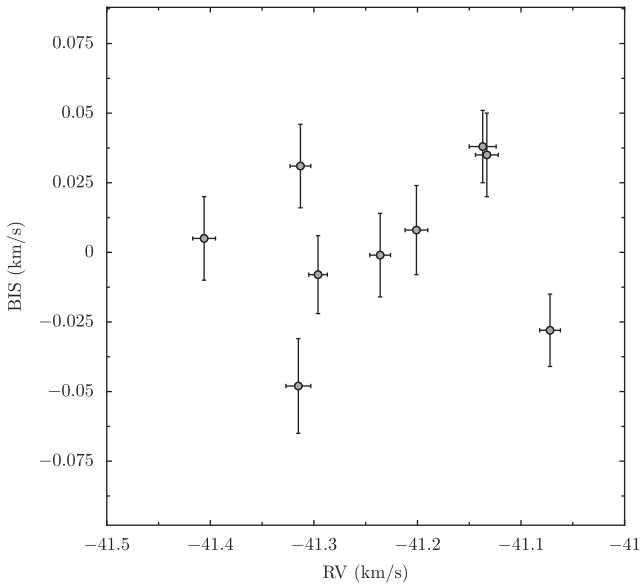

Figure 2. RV measurements versus the measured BIS in km s^{-1} obtained for our target star using the FEROS spectrograph. The correlation coefficient between these measurements is consistent with zero.

Table 1. Radial velocities obtained with the FEROS spectrograph along with the measured BIS.

Time (BJD UTC)	RV (km s^{-1})	σ_{RV}	BIS (km s^{-1})	σ_{BIS}
2457643.6804163	−41.315	0.012	−0.048	0.017
2457645.7862304	−41.236	0.010	−0.001	0.015
2457647.8755248	−41.133	0.011	0.035	0.015
2457700.7309840	−41.201	0.011	0.008	0.016
2457701.6407003	−41.313	0.010	0.031	0.015
2457702.7358066	−41.406	0.011	0.005	0.015
2457703.6386414	−41.296	0.009	−0.008	0.014
2457704.6259996	−41.137	0.013	0.038	0.013
2457705.6178241	−41.072	0.010	−0.028	0.013

$v\sin(i) = 2.06 \pm 0.77$ km s^{-1}, which make the host star a (slightly metal-rich) solar analogue.

In order to derive the radius, mass, age, luminosity and distance to the star, we used the latest version of the ISOCHRONES package (Morton 2015), which uses the derived atmospheric parameters along with photometric data in order to estimate them with evolutionary tracks. The photometric data for our star was obtained from different sources; these are presented in Table 2. We used the MESA Isochrones and Stellar Tracks (Choi et al. 2016; Dotter 2016) instead of the Darthmouth (Dotter et al. 2008) isochrones and stellar tracks, as the former cover wider ranges of radius, mass and age (although both gave results that were consistent within the errors). In order to explore the parameter space, the MULTINEST (Feroz, Hobson & Bridges 2009) algorithm as implemented in PyMultinest (Buchner et al. 2014) was used because it is well suited for problems like the one at hand, which are inherently degenerate. The derived stellar properties are presented in Table 2, all of which are consistent with the star being very similar to our own Sun ($R_* = 1.047^{+0.11}_{-0.08}$ R$_\odot$, $M_* = 1.007^{+0.040}_{-0.039}$, $L_* = 1.02^{+0.24}_{-0.18}$). As can be observed, the only parameter that significantly deviates (at 3σ) from that of a 'solar twin' is the metallicity which, as mentioned above, is slightly supersolar. We therefore consider the star a solar analogue.

Table 2. Stellar parameters of EPIC 220504338.

Parameter	Value	Source
Identifying information		
EPIC ID	220504338	EPIC
2MASS ID	01174783+0652080	2MASS
RA (J2000, h:m:s)	$01^h17^m47.829^s$	EPIC
Dec. (J2000, d:m:s)	$+06^o52'08.02''$	EPIC
RA p.m. (mas yr^{-1})	22.3 ± 1.7	UCAC4
Dec. p.m. (mas yr^{-1})	-15.8 ± 4.1	UCAC4
Spectroscopic properties		
$T_{\rm eff}$ (K)	5627 ± 88	ZASPE
Spectral Type	G	ZASPE
[Fe/H] (dex)	0.180 ± 0.062	ZASPE
$\log g_*$ (cgs)	4.400 ± 0.146	ZASPE
$v\sin(i)$ (km s^{-1})	2.06 ± 0.77	ZASPE
Photometric properties		
K_p (mag)	13.51	EPIC
B (mag)	14.445 ± 0.050	APASS
V (mag)	13.684 ± 0.030	APASS
g' (mag)	14.016 ± 0.030	APASS
r' (mag)	13.459 ± 0.020	APASS
i' (mag)	13.299 ± 0.030	APASS
J (mag)	12.347 ± 0.023	2MASS
H (mag)	11.998 ± 0.025	2MASS
Ks (mag)	11.949 ± 0.021	2MASS
Derived properties		
M_* (M$_\odot$)	$1.007^{+0.040}_{-0.039}$	ISOCHRONES[a]
R_* (R$_\odot$)	$1.047^{+0.11}_{-0.08}$	ISOCHRONES[a]
ρ_* (g cm^{-3})	$1.23^{+0.36}_{-0.32}$	ISOCHRONES[a]
L_* (L$_\odot$)	$1.02^{+0.24}_{-0.18}$	ISOCHRONES[a]
Distance (pc)	$553.4^{+59.0}_{-43.0}$	ISOCHRONES[a]
Age (Gyr)	$5.9^{+2.7}_{-3.4}$	ISOCHRONES[a]

Note. Logarithms are given in base 10.
[a]Using stellar parameters obtained from ZASPE.

3.2 Planet scenario validation

We performed a blend analysis following Hartman et al. (2011b,a), which attempts to model the available light curves, photometry calibrated to an absolute scale, and spectroscopically determined stellar atmospheric parameters, using combinations of stars with parameters constrained to lie on the Girardi et al. (2000) evolutionary tracks. Possible blend scenarios include blended eclipsing binary and hierarchical triple systems. The analysis includes fits of the secondary eclipses and out of transit variations using the photometric data. We find that the data are best described by a planet transiting a star. All of the above-mentioned blend scenarios are rejected at more than 5σ using the photometry alone. Including the RV data, the scenarios are further ruled out: the simulated RVs for the blend model that provides the best fit to the photometric data imply variations in RV of the order of 500 m s^{-1}, which are much higher than what we observe. Based on this analysis, we consider our planet validated.

It is important to note that with our validation procedures, we cannot rule out the possibility that the planetary transit is being diluted by a star within the 12 arcsec aperture radius used to obtain the *K*2 photometry. However, there is no known blending source within this radius in catalogues such as the *Gaia* Data Release 1 (Gaia Collaboration 2016) and UCAC4 (Zacharias et al. 2013), while there are some stars within the 12 arcsec aperture in the Sloan Digital Sky Survey which have $g > 20$, which would produce negligible dilutions in the *K*2 light curve.

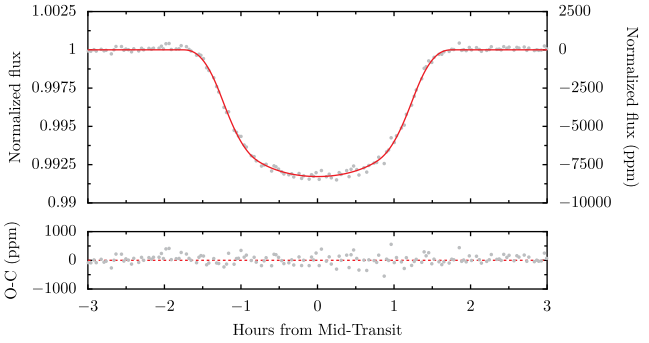

Figure 3. Phase-folded *K*2 photometry along with the best-fitting transit model obtained from the joint analysis performed with the EXONAILER algorithm.

3.3 Joint analysis

As in Brahm et al. (2016), the joint analysis of the *K*2 photometry and the FEROS RVs was performed using the EXOplanet traNsits and rAdIal veLocity fittER (EXONAILER; Espinoza et al. 2016) algorithm, which is available at GitHub.[4] The algorithm uses the BATMAN package (Kreidberg 2015) in order to perform the transit modelling, which has the advantage of allowing the usage of any limb-darkening law, which has been proven to be of importance if unbiased transit parameters are to be retrieved from high-precision photometry (Espinoza & Jordán 2015). As recommended in the study of Espinoza & Jordán (2015), we decided to let the limb-darkening coefficients be free parameters in the fit. Following the procedures outlined in Espinoza & Jordán (2016), we concluded that the square-root law is the optimal law to use in our case, as this is the law that retrieves the smaller mean-squared error (i.e. the best bias/variance trade-off) on the planet-to-star radius ratio, which is the most important parameter to derive for this exoplanet, as it defines the planetary density. The mean-squared error was estimated by sampling light curves with similar geometric, noise and sampling properties as the observed transit light curve, taking the spectroscopic information in order to model the real, underlying limb-darkening effect of the star. We sampled the coefficients of this law in our joint analysis using the efficient uninformative sampling scheme outlined in Kipping (2013). In order to take into account the smearing of the light curve due to the ∼27 min 'exposures' of the *Kepler* long-cadence observations, we use the selective resampling technique described in Kipping (2010) with $N = 20$ resampled points per data point in our analysis.

The RV analysis in our EXONAILER fit includes a RV jitter term that is added in quadrature to the measured uncertainties. We tried both circular and non-circular models, but computing the BIC-based evidence of both models, the non-circular model was indistinguishable from the circular one (the evidence for the non-circular model was ∼1.4 that of the circular model). As such, we decided to use the most parsimonious model of both, and fixed the eccentricity to zero. We note that the non-circular model allowed us to put a 3σ upper limit on the eccentricity of $e < 0.13$. Fig. 3 shows the phase-folded photometry along with the best-fitting model and Fig. 4 shows the RV measurements and the corresponding best-fitting model from our joint analysis. Table 3 presents the retrieved parameters. Note the moderate jitter of the star, of the order of $\sigma_{\rm RV} \sim 20\,{\rm m\,s^{-1}}$. As can be observed, the planet has a radius of $R_{\rm p} = 0.93^{+0.10}_{-0.07} R_{\rm J}$, and a mass of $M_{\rm p} = 1.29^{+0.13}_{-0.14} M_{\rm J}$, giving a density of $1.97^{+0.60}_{-0.53}\,{\rm g\,cm^{-3}}$

[4] https://github.com/nespinoza/exonailer

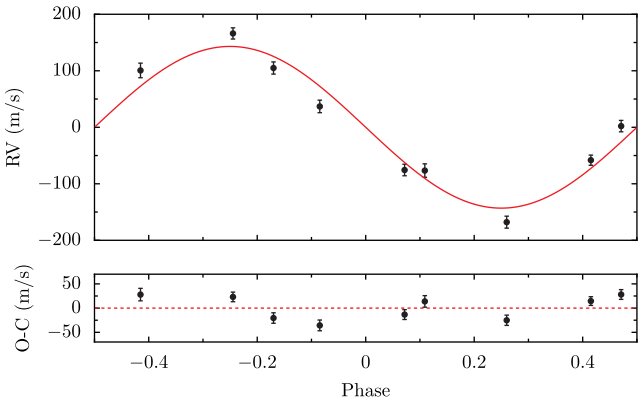

Figure 4. Phase-folded FEROS radial velocities along with the best-fitting model obtained from the joint analysis performed with the EXONAILER algorithm.

Table 3. Orbital and planetary parameters for K2-113.

Parameter	Prior	Posterior Value
Light-curve parameters		
P (d)	$\mathcal{N}(5.8177, 0.1)$	$5.817\,608^{+0.000\,031}_{-0.000\,029}$
$T_0 - 2450000$ (BJD)	$\mathcal{N}(7392.88575, 0.1)$	$7392.886\,05^{+0.000\,19}_{-0.000\,19}$
a/R_*	$\mathcal{U}(1, 15)$	$11.39^{+0.32}_{-0.32}$
$R_{\rm p}/R_*$	$\mathcal{U}(0.01, 0.2)$	$0.0911^{+0.000\,70}_{-0.000\,83}$
i (deg)	$\mathcal{U}(70, 90)$	$86.21^{+0.20}_{-0.21}$
$q_1{}^a$	$\mathcal{U}(0, 1)$	$0.72^{+0.17}_{-0.16}$
$q_2{}^a$	$\mathcal{U}(0, 1)$	$0.33^{+0.11}_{-0.15}$
σ_w (ppm)	$\mathcal{J}(10, 500)$	$138.4^{+1.8}_{-1.6}$
RV parameters		
$K\,({\rm m\,s^{-1}})$	$\mathcal{N}(0, 100)$	$144.5^{+13.5}_{-15.4}$
$\mu\,({\rm km\,s^{-1}})$	$\mathcal{N}(-41.24, 0.01)$	$-41.2375^{+0.0063}_{-0.0065}$
$\sigma_{\rm RV}\,({\rm m\,s^{-1}})$	$\mathcal{J}(1, 100)$	$24.3^{+10.1}_{-6.6}$
e	–	0 (fixed; upper limit[b] $e < 0.13$)
Derived parameters		
$s_1{}^a$	. . . . .	$0.30^{+0.20}_{-0.19}$
$s_2{}^a$	. . . . .	$0.55^{+0.26}_{-0.29}$
$M_{\rm p}$ ($M_{\rm J}$)	–	$1.29^{+0.13}_{-0.14}$
$R_{\rm p}$ ($R_{\rm J}$)	–	$0.93^{+0.10}_{-0.07}$
$\rho_p\,({\rm g\,cm^{-3}})$	–	$1.97^{+0.61}_{-0.53}$
$\log g_p$ (cgs)	–	$3.56^{+0.08}_{-0.10}$
a (AU)	–	$0.0558^{+0.0059}_{-0.0049}$
$\log \langle F \rangle$ (cgs)[c]	–	$8.640^{+0.033}_{-0.034}$
$V_{\rm esc}\,({\rm km\,s^{-1}})$ . . .	–	$69.7^{+4.9}_{-4.8}$
$T^d_{\rm eq}$ (K)		
Bond albedo of 0.0	–	1178^{+22}_{-23}
Bond albedo of 0.75	–	833^{+16}_{-16}

Note. Logarithms given in base 10. $\mathcal{N}(\mu, \sigma)$ stands for a normal prior with mean μ and standard deviation σ, $\mathcal{U}(a, b)$ stands for a uniform prior with limits a and b and $\mathcal{J}(a, b)$ stands for a Jeffrey's prior with the same limits. Times are given in BJD TDB.

[a]The q_1 and q_2 parameters are the triangular sampling coefficients used to fit for the square-root limb-darkening law (Kipping 2013). The s_1 and s_2 limb-darkening coefficients are recovered by the transformation $s_1 = \sqrt{q_1}(1 - 2q_1)$ and $s_2 = 2\sqrt{q_1}q_2$.

[b]3σ upper limit obtained from a non-circular joint fit to the data (see the text).

[c]Orbit averaged incident stellar flux on the planet.

[d]Full energy redistribution has been assumed.

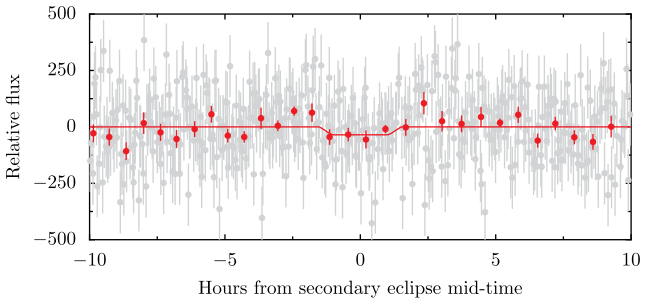

Figure 5. Secondary eclipse constrain using the *K*2 photometry (grey points; red points indicate binned data using 40-min bins in phase-space, which have median errorbars of 35 ppm per point). The best-fitting eclipse depth using this data (red solid line) is $F_p/F_* = 35.7^{+16.8}_{-19.0}$ ppm.

for this planet, which is on the high side when compared to a 'typical' hot-Jupiter (where $\rho_p \lesssim 1$ g cm^{-3}). We discuss these planetary parameters in the context of the discovered exoplanets in the next section.

3.4 Searching for additional signals in the *K*2 photometry

The *K*2 photometry was inspected in order to search for additional transiting planets, secondary eclipses and/or optical phase variations. After masking out the transits, the BLS algorithm was used in order to search for additional transiting planets, but no additional signals were found. Given the light curve precision is 138 ppm (Table 3), our data rule out any companion larger than $\sim$2 R$_\oplus$ at 3σ with periods $P \lesssim 39$ d. As for secondary eclipses, we ran an eclipse fit at the expected times, fixing all parameters except for the planet-to-star flux ratio, F_p/F_* and a time shift from the expected eclipse times from our circular model in order to allow departures from non-circularity present in the secondary eclipses (and not detected on our RV analysis). The result of our fit is presented in Fig. 5. The retrieved flux ratio in our fit was $F_p/F_* = 35.7^{+16.8}_{-19.0}$ ppm and the time shift from the expected secondary eclipse with our circular model (i.e. $T_0 - P/2$) was $-1.74^{+0.52}_{-0.24}$ h, which is consistent with a relatively weak detection of a secondary eclipse. This is interesting, however, as it allows us to put a constraint on the geometric albedo of the planet. Following Heng & Demory (2013), we estimate the geometric albedo of the planet as

$$A_g = \left[\frac{F_p}{F_*} - \frac{\pi \int_{\lambda_1}^{\lambda_2} B_\lambda(T_{eq})d\lambda}{F}\left(\frac{R_p}{R_*}\right)\right]\left(\frac{a}{R_p}\right)^2,$$

where F is the irradiation level at the substellar point calculated in Table 3 for our planet, $B_\lambda(T_{eq})$ is a blackbody of temperature T_{eq} (i.e. we approximate the thermal emission of the planet by a blackbody), with

$$T_{eq} = T_*\left(\frac{R_* f}{a}\right)^{1/2}(1 - A_B)^{1/4},$$

where f is the efficiency of heat redistribution from the dayside to the nightside of the planet and A_B is the Bond albedo. We assume a Lambertian sphere (i.e. isotropic scattering), so $A_B = 3A_g/2$ in our calculations. With this, we consider contributions from both reflected light (first term in the equation for A_g) and thermal emission (second term) from the planet. Integrating the blackbody from $\lambda_1 = 0.4$ μm to $\lambda_2 = 0.9$ μm (i.e. over the Kepler bandpass), we constrain the geometric albedo to be $A_g = 0.47^{+0.12}_{-0.16}$ if we assume complete heat redistribution (i.e. $f = 1/2$), and $A_g = 0.16^{+0.05}_{-0.06}$ if no redistribution is assumed (i.e. $f = 2/3$). These values are within the expected geometric albedos of other giant planets measured by the *Kepler* spacecraft (see e.g. Heng & Demory 2013; Angerhausen, DeLarme & Morse 2015). Fixing the time shift to zero gives the same constraint on the geometric albedo. Optical phase variations were not detected in the light curve.

4 DISCUSSION

Fig. 6 puts the newly discovered planet in the context of the population of known hot-Jupiters in the mass–radius diagram (left-hand panel, $P \lesssim 10$ d, $M \gtrsim 0.1 M_J$) and of the known hot and warm Jupiters in the equilibrium temperature–radius diagram (right-hand panel). As can be observed, K2-113 falls on a region in the mass–radius diagram that is currently not very well populated, and which hosts the densest hot-Jupiters with masses below $2M_J$ ($\sim$2 g cm^{-3}). In the equilibrium temperature–radius diagram, on the other hand, it falls on the typical sizes of warm Jupiters, despite the fact that K2-113 would be typically classified as being 'hot' due to its orbit-averaged flux of $\langle F \rangle = 4 \times 10^8$ erg cm^{-2} s^{-1}, which is above (but very close to) the 2×10^8 erg cm^{-2} s^{-1} threshold where it is believed 'inflation' mechanisms of giant planets stop being important (Demory & Seager 2011; Miller & Fortney 2011). Using the relations of Enoch, Collier Cameron & Horne (2012), K2-113 would be expected to have a radius of $\sim 1.11 R_J$, which is anyway consistent (at 2σ) with the measured radius.

The mass and radius of K2-113 could be explained in terms of the amount of heavy elements in the planet. In Fig. 6, we see that our planet falls just where the planet evolution models of Fortney et al. (2007) predict it to be if it had a 100M$_\oplus$ core, which is a proxy for the amount of heavy elements in the planet. Of course, giant planets are probably not just H/He envelopes sitting on top of a heavy-element core. As shown by Thorngren et al. (2016), heavy-element enrichment of the envelope is also a very important factor to take into account, although difficult to estimate based on planetary mass alone due to the high scatter in the planetary mass–heavy element relation derived in that work, which is both due to the errors on the masses, radii and ages of the planets used to derive that relation, and the stochasticity of the planet formation process, which allow for planets of similar mass to have inherently different heavy-element content. For example, using this relation, where a 10 M$_\oplus$ heavy-element core is assumed, the amount of heavy elements present in the envelope of K2-113 could be anywhere from $\sim$30 M$_\oplus$ to $\sim$120 M$_\oplus$ at 1σ.

Instead of trying to estimate the heavy element mass in K2-113 directly, which is rather hard to do due to the possibility that inflation could be impacting on K2-113's radius, we can compare it in terms of its radius and mass to the 'warm' Jupiter WASP-130b ($M_p = 1.23 \pm 0.04 M_J$ and $R_p = 0.89 \pm 0.03 R_J$; Hellier et al. 2017). This comparison is interesting because WASP-130b is probably not affected by any inflation mechanisms due to its relatively low irradiation level ($\log \langle F \rangle = 10^8$, with F in cgs units). Because of this, Thorngren et al. (2016) were able to use structure models in order to estimate a heavy-element mass of $\sim$110 M$_\oplus$ for WASP-130b based on its mass, radius and age. Assuming that the ages of both systems are similar, we can use the heavy-element mass estimated for WASP-130b as a lower limit on the heavy-element mass of K2-113. This is because, as discussed above, K2-113 is within the regime where inflation mechanisms are expected to act, and, thus, the observed radius of K2-113 should be larger to what contraction models as the ones used by Thorngren et al. (2016) would predict for its heavy-element mass, total mass and age. Following this logic,

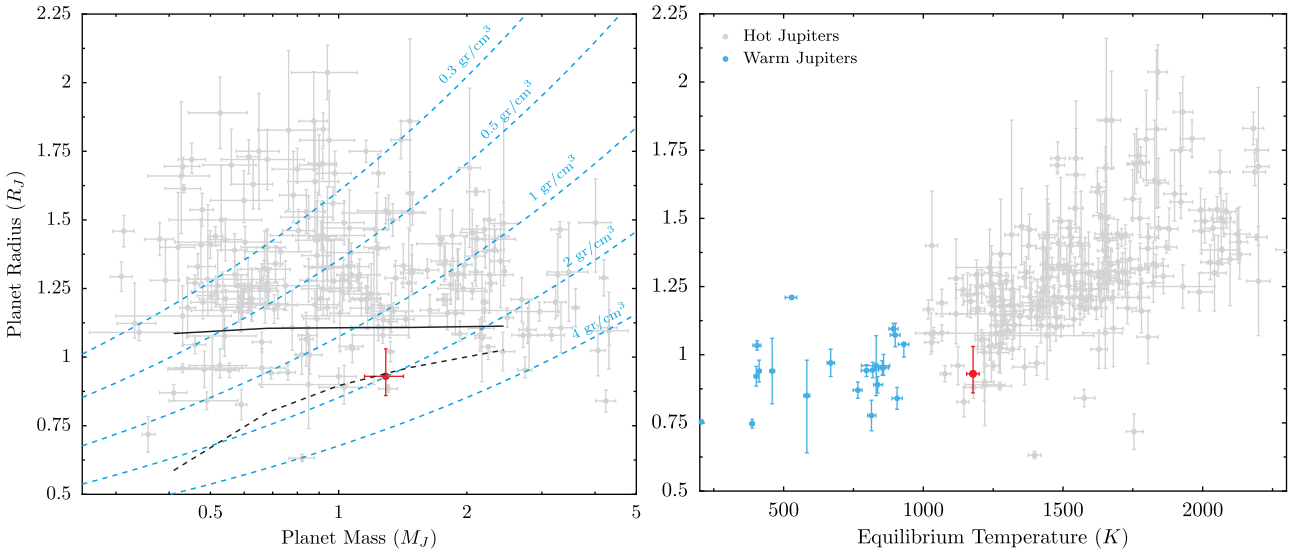

Figure 6. *Left.* Mass–radius diagram for known hot-Jupiters (grey points), along with iso-density curves (blue dashed lines) and the expected mass–radius relation for 4.5 Gyr planets at 0.045 au from the Sun with no core (black, dashed line) and a 100 $M_\oplus$ core (black, solid line). K2-113 is indicated as the red point with errorbars. *Right.* Equilibrium temperature–radius diagram of known hot-Jupiters (grey points) and warm Jupiters (blue points), for comparison. Again, K2-113 is depicted as a red point with errorbars.

if K2-113's radius without this inflation mechanism were, say, the radius of WASP-130b, then with inflation the observed radius of K2-113 should be larger than WASP-130b's. This is why the estimated heavy-element content on WASP-130b is a lower limit on the heavy element content of K2-113 – of course assuming the observed mass, radius and age of both planets are indistinguishable; a reasonable assumption given the error bars on those properties.

Following a similar logic to the one used above, we can also estimate an upper limit on the heavy element content of K2-113 by comparing it to CoRoT-13b ($M_p = 1.31 \pm 0.07$ and $R_p = 0.885 \pm 0.014$; Cabrera et al. 2010), which is the closest planet in mass and radius to K2-113 among the known hot-Jupiters, despite the fact that the former orbits a hotter star and hence, has a larger equilibrium temperature (1700 K). This difference again could be explained (if we assume again the system ages, masses and radii are indistinguishable) in terms of the amount of heavy elements in these planets, with K2-113 having a lower amount than CoRoT-13b, which is estimated to have between ∼140 and 300 $M_\oplus$ of heavy elements.

The difference in heavy element content between WASP-130b, K2-113 and CoRoT-13b would most likely be a signature of their different formation histories rather than a correlation with other physical parameters of the system, such as the metallicities of the parent stars, whose correlation with the heavy element content on a given planet is rather weak (Thorngren et al. 2016). In fact, in this case the metallicity of WASP-130 is the largest of the three, while the metallicity of CoRoT-13 is the smallest, which casts further doubts on the prediction power of such a correlation if it were to exist.

5 CONCLUSIONS

In this work, we have presented the discovery of K2-113, a new hot-Jupiter orbiting a slightly metal-rich solar analogue discovered using photometry from Campaign 8 of the *K*2 mission and follow-up radial velocities using the FEROS spectrograph. The planet has a radius of $R_p = 0.91^{+0.10}_{-0.07} R_J$, and a mass of $M_p = 1.28^{+0.11}_{-0.12} M_J$. With a density of $2.08^{+0.66}_{-0.57}$ g cm^{-3}, the planet is denser than most hot-Jupiters with masses under $2M_J$. We explain its mass and radius in terms of the amount of heavy elements in the planet, which should be of the order of ∼110 $M_\oplus$ or greater.

ACKNOWLEDGEMENTS

We would like to thank R. Luger for sharing the EVEREST light curves for the exoplanet presented in this work as soon as they were available, and an anonymous referee for her/his comments that greatly improved the presented work. NE is supported by the CONICYT-PCHA/Doctorado Nacional graduate fellowship. NE, RB, AJ and CC acknowledge support from the Ministry for the Economy, Development, and Tourism Programa Iniciativa Científica Milenio through grant IC 120009, awarded to the Millennium Institute of Astrophysics (MAS). AJ acknowledges support from FONDECYT project 1171208 and from BASAL CATA PFB-06. Support for CC is provided by Proyecto FONDECYT Iniciación a la Investigación 11150768. This paper includes data collected by the K2 mission. Funding for the K2 mission is provided by the NASA Science Mission directorate.

REFERENCES

Angerhausen D., DeLarme E., Morse J. A., 2015, PASP, 127, 1113
Bakos G., Noyes R. W., Kovács G., Stanek K. Z., Sasselov D. D., Domsa I., 2004, PASP, 116, 266
Bakos G. Á. et al., 2013, PASP, 125, 154
Baraffe I., Chabrier G., Barman T. S., Allard F., Hauschildt P. H., 2003, A&A, 402, 701
Borucki W. J. et al., 2010, Science, 327, 977
Brahm R. et al., 2015, AJ, 150, 33
Brahm R. et al., 2016, PASP, 128, 124402
Brahm R., Jordán A., Espinoza N., 2017a, PASP, 129, 034002
Brahm R., Jordan A., Hartman J., Bakos G., 2017b, MNRAS, 467, 971
Buchner J. et al., 2014, A&A, 564, A125
Cabrera J. et al., 2010, A&A, 522, A110
Choi J., Dotter A., Conroy C., Cantiello M., Paxton B., Johnson B. D., 2016, ApJ, 823, 102

Crossfield I. J. M. et al., 2016, ApJS, 226, 7
Demory B.-O., Seager S., 2011, ApJS, 197, 12
Dotter A., 2016, ApJS, 222, 8
Dotter A., Chaboyer B., Jevremović D., Kostov V., Baron E., Ferguson J. W., 2008, ApJS, 178, 89
Enoch B., Collier Cameron A., Horne K., 2012, A&A, 540, A99
Espinoza N., Jordán A., 2015, MNRAS, 450, 1879
Espinoza N., Jordán A., 2016, MNRAS, 457, 3573
Espinoza N. et al., 2016, ApJ, 830, 43
Feroz F., Hobson M. P., Bridges M., 2009, MNRAS, 398, 1601
Fortney J. J., Marley M. S., Barnes J. W., 2007, ApJ, 659, 1661
Gaia Collaboration, 2016, A&A, 595, A2
Girardi L., Bressan A., Bertelli G., Chiosi C., 2000, A&AS, 141, 371
Hartman J. D. et al., 2011a, ApJ, 728, 138
Hartman J. D. et al., 2011b, ApJ, 742, 59
Hellier C. et al., 2017, MNRAS, 465, 3693
Heng K., Demory B.-O., 2013, ApJ, 777, 100
Jordán A. et al., 2014, AJ, 148, 29
Kaufer A., Pasquini L., 1998, in D'Odorico S., ed., Proc. SPIE Conf. Ser. Vol. 3355, Optical Astronomical Instrumentation. SPIE, Bellingham, p. 844
Kipping D. M., 2010, MNRAS, 408, 1758
Kipping D. M., 2013, MNRAS, 435, 2152
Kovács G., Zucker S., Mazeh T., 2002, A&A, 391, 369
Kovács G. et al., 2010, ApJ, 724, 866
Kreidberg L., 2015, PASP, 127, 1161
Luger R., Agol E., Kruse E., Barnes R., Becker A., Foreman-Mackey D., Deming D., 2016, AJ, 152, 100
Luger R., Kruse E., Foreman-Mackey D., Agol E., Saunders N., 2017, AJ, preprint (arXiv:1702.05488)
Miller N., Fortney J. J., 2011, ApJ, 736, L29
Morton T. D., 2015, Astrophysics Source Code Library, record ascl:1503.010
Pollacco D. L. et al., 2006, PASP, 118, 1407
Thorngren D. P., Fortney J. J., Murray-Clay R. A., Lopez E. D., 2016, ApJ, 831, 64
Zacharias N., Finch C. T., Girard T. M., Henden A., Bartlett J. L., Monet D. G., Zacharias M. I., 2013, AJ, 145, 44

This paper has been typeset from a TEX/LATEX file prepared by the author.